Journal of Chromatography A 1734 (2024) 465261

Contents lists available at ScienceDirect

Journal of Chromatography A

journal homepage: www.elsevier.com/locate/chroma

Mechanistic modeling of minute virus of mice surrogate removal by anion exchange chromatography in micro scale

Lukas Döring [a,b], Johannes Winderl [a], Matthias Kron [a], Jürgen Hubbuch [b,*]

[a] *Process Science, Rentschler Biopharma SE, Erwin-Rentschler-Str. 21 88471 Laupheim, Germany*
[b] *Karlsruhe Institute of Technology (KIT), Institute of Engineering in Life Sciences, Section IV: Biomolecular Separation Engineering, Fritz-Haber-Weg 2 76131 Karlsruhe, Germany*

ARTICLE INFO

Keywords:
Viral clearance
Mechanistic modeling
Anion exchange chromatography
Minute virus of mice (MVM)
MVM mock virus particle (MVP)

ABSTRACT

Biopharmaceutical products are often produced in Chinese hamster ovary (CHO) cell cultures that are vulnerable to virus infections. Therefore, it is a regulatory requirement that downstream purification steps for biopharmaceuticals can remove viruses from feedstocks. Anion exchange chromatography (AEX) is one of the downstream unit operations that is most frequently used for this purpose and claimed for its capability to remove viruses. However, the impact of various process parameters on virus removal by AEX is still not fully understood. Mechanistic modeling could be a promising way to approach this gap, as these models require comparatively few experiments for calibration. This makes them a valuable tool to improve understanding of viral clearance, especially since virus spiking studies are costly and time consuming.

In this study, we present how the virus clearance of a MVM mock virus particle by Q Sepharose FF resin can be described by mechanistic modeling. A lumped kinetic model was combined with a steric mass action model and calibrated at micro scale using three linear gradient experiments and an incremental step elution gradient. The model was subsequently verified for its capability to predict the effect of different sodium chloride concentrations, as well as residence times, on virus clearance and was in good agreement with the LRVs of the verification runs. Overall, models like this could enhance the mechanistic understanding of viral clearance mechanisms and thereby contribute to the development of more efficient and safer biopharmaceutical downstream processes.

1. Introduction

Downstream processing of biopharmaceuticals is a complex process consisting of several sequential unit operations. While filtration steps are often used for clarification, bioburden control or concentration of intermediates, chromatography steps contribute by removing the majority of product- and process-related impurities. Since the chromatography steps play such a crucial role in producing pure protein drug substance, a lot of work has been put into understanding and optimization of affinity (e.g. Protein A), anion exchange (AEX), and cation exchange (CEX) chromatography. These efforts led to approaches allowing the *in-silico* development and optimization of such purification steps. In the past years, mechanistic modeling of chromatography steps gained more and more interest. These models describe the behavior of chromatography steps based on physical and chemical laws and can predict a wide range of experimental conditions with a (comparatively) limited number of wet lab experiments. Especially the behavior of product-related impurities like HMWS, LMWS and charge variants, but also the performance of whole process trains, have been shown to be described accurately by these models [1–3]. However, process-related impurities such as host cell proteins and DNA still pose a challenge, and mechanistic modeling approaches for virus removal are currently limited to virus filtration [4,5]. The ultimate goal is thus to extend product related process models [3] with their capability to handle virus removal.

Biopharmaceutical products like monoclonal antibodies and so-called designer proteins are often produced in chinese hamster ovary (CHO) cell cultures. Since mammalian cell cultures like CHOs produce retrovirus like particles (RVLPs) and are vulnerable to virus infections, viral clearance is a regulatory requirement for clinical stages as well as market authorization of biopharmaceuticals (ICHQ5A) [6–8]. Apart from dedicated process steps (e.g. virus inactivation and virus filtration), chromatography steps like protein A, AEX and CEX are frequently tested for their ability to remove viruses [9,10]. AEX chromatography has been shown to be robust and effective in clearing enveloped retroviruses as

---

* Corresponding author at: Fritz-Haber-Weg 2 76131 Karlsruhe, Germany.
E-mail address: juergen.hubbuch@kit.edu (J. Hubbuch).

https://doi.org/10.1016/j.chroma.2024.465261
Received 5 June 2024; Received in revised form 2 August 2024; Accepted 11 August 2024

well as non-enveloped parvoviruses [11–13]. Like most biopharmaceutical proteins, monoclonal antibodies possess neutral to basic pIs [14], while viruses have more acidic charge characteristics with pIs ranging from 3.5 to 7 [15]. Therefore, AEX is often operated in flow-through mode at a pH below the pI of the protein of interest. Under these conditions the product flows through the column while viruses are adsorbed by the resin via electrostatic interactions [12].

Due to the cost and time intensive nature of viral clearance studies, they are often limited to the required minimum and an in-depth characterization of viral clearance behavior is rarely performed [13,16,17]. Viral clearance studies are usually performed with material obtained from the initial manufacturing scale runs. Insufficient removal and inactivation can potentially lead to rejection of production lots and another time-consuming development cycle. The high impact of failed viral clearance studies and the lack of mechanistic understanding can result in processes where yield and purity are sacrificed to ensure sufficient viral clearance.

The developments in mechanistic modeling are accompanied by the availability of methodologies using highly characterized retrovirus-like particles (RVLP), bacteriophages, or minute virus of mice mock virus particles (MVP) in combination with PCR and ELISA methods [18–21]. These methodologies allow virus removal studies under Biosafety Level 1 (BSL 1), thereby enabling the investigation of viral clearance at reasonable cost and throughput. This already led to an increase in the mechanistic understanding of chromatography, inactivation, and virus filtration steps dedicated for virus clearance [20,22–26].

Although in the past years the understanding of virus removal by AEX chromatography was mainly driven by statistical models or molecular modeling [13,22,27], approaches to model interactions between viruses and ion exchange resins are known to be valuable for determination of isoelectric points by chromatofocusing [28]. However, mechanistic models combining both column and adsorption models to predict virus removal on ion exchange chromatography resins have not been published so far.

In this study, we introduce mechanistic modeling as a tool to describe the virus removal of MVP using a Q Sepharose FF (QSFF) resin. A steric mass action (SMA) adsorption isotherm was calibrated with three linear gradient experiments (LGE) with different gradient lengths and an incremental step elution (ISE) gradient using a micro scale column. An asymmetric sampling approach was applied to achieve sufficient resolution in order to describe the chromatographic behavior on the $\log_{10}$ scale. The model was subsequently verified for its capability to predict the effect of different sodium chloride concentrations and residence times. The model and verification runs showed good agreement and comparable logarithmic reduction values (LRVs) for effective (LRV $>$ 4), moderate (LRV 1 - 4) and insignificant virus removal (LRV $<$ 1).

2. Theory

2.1. Column and system model

In this study, a lumped kinetic model (LKM) was used. LKMs neglect pore diffusion as well as film mass transfer and allow the definition of molecule-specific porosities ($\varepsilon_{t,i}$). Therefore, LKMs are particularly useful in describing chromatography processes where the effective mass transfer does not pose a limitation and molecules have different pore accessibility. Eq. (1) describes the LKM where the temporal change in concentration of the i th solute is dependent on convective mass transport driven by volumetric flow with the interstitial velocity u_{int}. The interstitial velocity is described by $u_{int} = u_{lin} / \varepsilon_b$ were u_{lin} is the linear flow rate and ε_b is the interstitial porosity. Peak broadening effects are described by an apparent dispersion coefficient D_{app}. To consider the effect of the flowrate on the dispersion D_{app} was assumed to depend on the interstitial velocity via a second order polynomial Eq. (2). The model is complemented by Danckwerts boundary conditions in Eq. (3) and (4) with $c_{in,i}(t)$ being the concentration of the i th solute at the column inlet. Mixing behavior of the chromatography system used was represented by continuously stirred tank reactors (CSTR) as defined in Eq. (5) with u_{vol} being the volumetric flow rate and V_{CSTR} being the mixer volume and a dispersed plug flow reactor (DPFR) as defined in Eq. (6) with the linear velocity u_{lin} and the axial dispersion D_{ax}.

$$\frac{\partial c_i}{\partial t}(x,\ t) = -u_{int}(t)\frac{\partial c_i}{\partial x}(x,t) + D_{app}\frac{\partial^2 c_i}{\partial x^2}(x,t) - \frac{1-\ \varepsilon_{t,\ i}}{\varepsilon_{t,\ i}}\ \frac{\partial q_i}{\partial} \tag{1}$$

$$D_{app} = D_{app,\ const.}\ + D_{app,\ lin.}\ u_{int} + D_{app,sqrd.}\ \ {u_{int}}^2 \tag{2}$$

$$\frac{\partial c_i}{\partial t}(0,\ t) = \frac{u_{int}(t)}{D_{app,\ i}}\left(c_i(0,\ t) - c_{in,i}(t)\right) \tag{3}$$

$$\frac{\partial c_i}{\partial t}(L,\ t) = 0 \tag{4}$$

$$\frac{\partial c_i}{\partial t}\ =\ \frac{u_{vol}}{V_{CSTR}}\ (c_{in} - c_{CSTR}) \tag{5}$$

$$\frac{\partial c_{DPRF}}{\partial t}\ = -u_{lin}\ \frac{\partial c_{DPFR}}{\partial x} + D_{ax}\frac{\partial^2 c_{DPFR}}{\partial x^2} \tag{6}$$

2.2. Steric mass action isotherm

To model the electrostatic adsorption to the resin the steric mass action (SMA) isotherm was used. The SMA isotherm describes ion exchange chromatography as a non-linear competitive equilibrium between an adsorbed particle concentration in the solid and liquid phase denoted by q_i and $c_{p,i}$ and the salt concentration c_s using a stochiometric approach. The characteristic charge ν depicts the number of functional groups used up for electrostatic interaction, while the steric shielding factor σ describes the additional number of functional groups sterically occupied by the adsorbing molecule. The shielding factor σ was neglected since it was assumed to be not limiting at the MVP load densities used in this study. The total ionic capacity of the respective resin is described by Λ [29]. The kinetic form of the SMA introduced by Hahn et al. (Eq. (7)) was used describing the adsorption rate and desorption rate of the i th solute as $k_{eq,i} = k_{ads,i}/k_{des,i}$ and $k_{kin,i} = 1/k_{des,i}$ respectively [30].

$$k_{kin,i} = k_{eq,\ i}\left(\Lambda - \sum_{j=1}^{k}(\nu_j + \sigma_j)q_j\right)^{\nu_i} c_{p,i} - q_i {c_s}^{\nu_i} \tag{7}$$

$$q_{salt} = \Lambda - \sum_{j=1}^{k}\nu_j q_j \tag{8}$$

2.3. Calculation of logarithmic reduction values (LRV)

As defined in ICHQ5a the MVP logarithmic reduction values (LRVs) were calculated considering the virus titers and volumes of the preprocessed and post processed solutions [6]. The volume and concentration of MVP in the preprocessed solution are given as $V_{MVP,pre}$ and $c_{MVP,pre}$ respectively, while the volume and concentration of the post processed solution are given as $V_{MVP,post}$ and $c_{MVP,post}$ (Eq. (9)).

$$LRV = log_{10}\left(V_{MVP,pre} * \ c_{MVP,pre}\right) - log_{10}\left(V_{MVP,post} * \ c_{MVP,post}\right) \tag{9}$$

3. Materials and methods

3.1. Resin, buffers and molecules

If not stated otherwise all chemicals were obtained from Merck (Darmstadt, Germany). The strong anion exchange chromatography resin Q Sepharose FF (QSFF) (Cytiva, Marlborough, USA) was used in this study. The LKM model was calibrated in micro scale using MiniCrom

Prepacked columns (Repligen) with an inner diameter (d_c) of 5 mm and bed height (L_c) of 10 mm. In the following this column type is named micro scale column. Spiking MVP were commercially obtained (Cygnus, Southport, USA).

Chromatography runs for calibration and validation were performed with a multi component buffer system (MCBS) consisting of 20 mM acetate, 20 mM HEPES, 20 mM MES and 20 to 1000 mM NaCl. Buffers were prepared with purified water, pH adjusted to 7.5 using 1 M sodium hydroxide or 1 M hydrochloric acid and filtered using 0.45/0.22 µm Sartopore 2 (Sartorius, Göttingen, Germany) prior to use.

3.2. Instruments

Chromatographic experiments were carried out using an ÄKTA Pure 25 system equipped with 10 mm UV flow cell and an F9-C fraction collector. The chromatography system was operated with Unicorn 7.10 (Cytiva, Marlborough, USA). Tubing configuration of the chromatography system conforms to the configuration described by Schweiger et al. [31].

3.3. Software

Simulations and parameter estimation were performed using GoSilico chromatography modeling software (GSCM) (Cytiva, Marlborough, USA) a commercially available software for numerical simulation of chromatography processes based on mechanistic models. For all simulations columns were spatially discretized into 30 axial cells of the same length. For temporal discretization a Crank-Nicolson time stepping scheme with a step size of 1 s was used. Python version 3.7.6 was used for data visualization.

3.4. System and column characterization

System specific sensor dead volumes were estimated by pulse injections with 1 % (v/v) acetone or 1 M sodium chloride using water for injection (WFI) as running buffer. System mixing behavior was modeled with a continuously stirred tank reactor (CSTR). System $CSTR_{post}$ behavior was determined from the conductivity traces of step transition experiments from 100 mM sodium chloride to 0.5 % (v/v) acetone and 300 mM sodium chloride at 0.33, 0.66, 1.00, 1.33, 1.66 and 2.00 mL/min. For determination of post column dispersive plug flow reactor (DPFR) dispersion pulse experiments were performed injecting 0.01 mL of spiking MVP with a concentration of 10^{12} MVP/ mL at flow rates of 0.66 and 1.66 mL/min. $CSTR_{pre}$ behavior was determined with a 10 mL linear gradient from WFI to 500 mM sodium chloride. To take account for the flow rate dependence of the mixing behavior CSTR characterization was performed at volumetric flow rates of 0.33, 0.66, 1.00, 1.33, 1.66 and 2.00 mL/min.

Total porosity ε_t and interstitial porosity ε_b were determined with 1 M sodium chloride pulse as pore penetrating tracer and MVP in 1 M sodium chloride as none pore penetrating tracer. Column band broadening in dependence of the interstitial flow rate u_{int} was derived from the empirical correlation for minichrom columns published by Schweiger et al. (Eq. (10)) with D_0 being the diffusion coefficient, r_p being the particle radius and the column diameter d_c and transformed to the apparent dispersion (D_{app}) factor using Eq. (11) obtained from Schimdt-Traub et al. [32]. Combining and rearranging Eq. (10) and Eq. (11) results in Eq. (12). Assuming that D_{app} cannot become lower than D_0 Eq. (13) can be derived, which represents the second order polynomial of Eq. (2) introduced in Section 2.1.

$$\frac{\sigma_{col}^2}{d_c^3} = 0.00681 * L^{0.549} + 2.31 * 10^{-5} * L * \frac{u_{int} \;*\; \varepsilon_b \;*\; 2r_p}{D_0} \tag{10}$$

$$D_{app} = \frac{1}{2} L \, u_{int} \left(\frac{\sigma_{col}}{V_{int}}\right)^2 \tag{11}$$

$$D_{app} = \frac{0.00681 * L^{1.549} * d_c^3}{2 \, V_{int}^2} u_{int} + \frac{2.31 * \; 10^{-5} * L^2 * d_c^3 * \varepsilon_b * 2r_p}{2 \, V_{int}^2 \, D_0} u_{int}^2 \tag{12}$$

$$D_{app} = D_0 + \frac{0.00681 * L^{1.549} * d_c^3}{2 \, V_{int}^2} u_{int} + \frac{2.31 * \; 10^{-5} * L^2 * d_c^3 * \varepsilon_b * 2r_p}{2 \, V_{int}^2 \, D_0} u_{int}^2 \tag{13}$$

All system and column characterization experiments were performed in triplicates.

3.5. Chromatography experiments and parameter estimation

The isotherm parameters k_{eq} and ν of the SMA were initially estimated from UV280 traces of three linear gradients (50, 100 and 150 CV) from 20 mM to 1000 mM sodium chloride. The kinetic parameter k_{kin} was estimated from the linear gradient runs and an additional run with incremental step elution (ISE) via inverse estimation using the GSCM software. For inverse estimation UV280 trace as well as offline data generated with the Immuno-qPCR were used. Blank runs without MVP were performed for each run and the UV280 trace was subtracted from each of the calibration runs before parameter estimation. For all runs load and wash fractions were collected as a pool. Peaks of the LGE runs were sampled asymmetrically with a volume per fraction of 0.2 mL at conductivities between 24 – 26 mS/cm while 0.6 mL per fraction were collected at conductivities > 24 mS/cm. For the increment steps 15 mL were collected per step.

Table 1 shows load material composition, flowrates and NaCl concentration of the respective Equilibration, Wash and Elution steps, as well as the objective of the chromatography runs performed during this study. Uncertainty of the model parameters was evaluated based on an estimate of the covariance matrix as previously described in Hahn et al. [33]. Confidence bands for model verification were estimated based on a sampling of a multivariate normal distribution with mean equal to the parameter estimate of the respective parameter and the estimated covariance matrix using the GSCM software. For verification of the impact of sodium chloride on LRVs 500 simulations were performed per 20 mM sodium chloride increment. For residence time-LRV dependence 500 simulations were performed at residence times of 1.0, 3.6, 7.2, 18.0, 24.0, 36.0, 72.0, and 144.0 s. The simulated method consisted of a 5 mL load with a concentration of 2×10^{10} MVP/mL and a 10 mL isocratic wash step with the respective sodium chloride concentration. For calculation of LRVs the MVP contained in flowthrough and wash fractions were determined.

3.6. Virus surrogate quantification

MVP was quantified via Immuno-qPCR using the MockV® MVM Kit (Cygnus, Southport, USA). To perform the immunoassay samples were applied to a 96-well plate coated with antibodies targeting MVPs. After 30 min of incubation at 37 °C plates were washed, and a DNA conjugated detector antibody was applied. After intensively washing of the plate the DNA was dissociated from the antibody using the respective buffer as previously described in [20]. The resulting samples were prepared and quantified according to the instructions of the vendor using a Light Cycler® 480 II device (Roche). Lower limit of quantification (LOQ) was set to 5×10^5 MVP/mL which was the lowest concentration of the standard curve that could be reliably distinguished from the background signal.

4. Results

4.1. System and column characterization

Since it is known that extra column band broadening can become dominant for very small columns [31], an in depth characterization of

Table 1
Summary of calibration and verification experiments performed with different gradients, flow rates and sodium chloride concentrations.

						NaCl conc. c_s [mM]		
Load conc. [MVP/mL]	Load volume [mL]	Objective	Flow rate [cm/h]	Residence time [s]	Elution mode	Load / Equilibration / Wash	Elution	Gradient / Step length[CV]
2×10^{10}	5	Yamamoto method	200	18.0	LGE	20	20 – 1000	50, 100, 150
2×10^{10}	5	Inverse estimation	200	18.0	ISE	20	100 – 320	50
2×10^{10}	5	Verification NaCl	200	18.0	FT	20	–	–
2×10^{10}	5	Verification NaCl	200	18.0	FT	120	–	–
2×10^{10}	5	Verification NaCl	200	18.0	FT	140	–	–
2×10^{10}	5	Verification NaCl	200	18.0	FT	160	–	–
2×10^{10}	5	Verification NaCl	200	18.0	FT	180	–	–
2×10^{10}	5	Verification NaCl	200	18.0	FT	200	–	–
2×10^{10}	5	Verification NaCl	200	18.0	FT	220	–	–
2×10^{10}	5	Verification NaCl	200	18.0	FT	240	–	–
2×10^{10}	5	Verification flow rates	25	144.0	FT	20	–	–
2×10^{10}	5	Verification flow rates	50	72.0	FT	20	–	–
2×10^{10}	5	Verification flow rates	100	36.0	FT	20	–	–
2×10^{10}	5	Verification flow rates	200	18.0	FT	20	–	–
2×10^{10}	5	Verification flow rates	500	7.0	FT	20	–	–

the chromatography system was performed. As shown in Fig. 1, the components of the ÄKTA Pure 25 system were lumped into mixing behavior before the column $CSTR_{pre}$ and after the column $CSTR_{post}$. A post column DPFR was simulated to take account for the molecule specific dispersive behavior of the MVP. Additionally, delays were considered to describe the dead volumes of valves and tubing of the system.

The factors of the system specific $CSTR_{post}$ were determined by bypassing pre and post column tubing and applying an acetone sodium chloride mixture through the injection valve. A delay between UV and conductivity sensor of 0.086 mL was determined. As shown in Fig. 1B-D, a $CSTR_{post}$ of 0.080 mL was reversely fitted from the conductivity traces. To examine whether the mixing behavior of $CSTR_{post}$ is considerably flow dependent these experiments were performed at 0.33, 0.66, 1.00, 1.33, 1.66 and 2.00 ml/min. However, with increasing flow rates the onset of the conductivity traces was shifted towards higher delays. To take this shift into account a linear term was introduced to describe $delay_{post}$ in dependence of the volumetric flowrate u_{vol} (Fig. 2B-C). Further, pulse experiments were performed at 0.66 mL/min and 1.66 mL/min to consider the specific dispersion of MVP throughout the system. As shown in Fig. 3A, the MVP showed higher dispersion than predicted from the small molecule tracers alone. To take this into account, a post column DPFR was included with an axial dispersion D_{ax} of 1.3×10^4 mm^2/s was inversely estimated. The MVP pulse at the lower flowrate showed signs of deformation at the onset of the peak. Nevertheless, the introduction of one none flow dependent DPFR sufficiently described peak broadening and tailing parameter of MVP pulses at both flow rates (Fig. 3B).

In the next step, $CSTR_{pre}$ was calibrated using a linear sodium chloride gradient at 0.33, 0.66, 1.00, 1.33, 1.66 and 2.00 ml/min. As shown in Fig. 2A, mixing behavior could be described well combining a 0.095 mL $CSTR_{pre}$ with a 1.43 mL $delay_{pre}$ and no additional flow dependent delay was necessary. All flow rates showed a similar mixing behavior and were well described by $CSTR_{pre}$. System components, lumped components described by the model, and volumes of the respective CSTRs and delays are shown in Fig. 1.

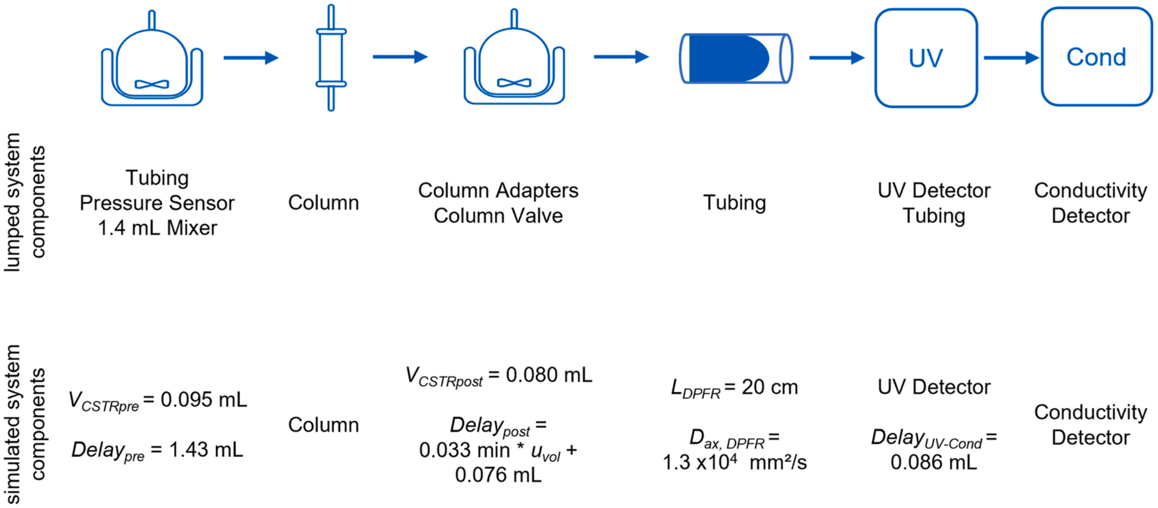

Fig. 1. Configuration and characterization of ÄKTA Pure 25 components. For simulation mixing behaviour of system components were lumped into two mixers $CSTR_{pre}$, $CSTR_{post}$ and a DPFR. Additionally delays were included to consider hold up volumes.

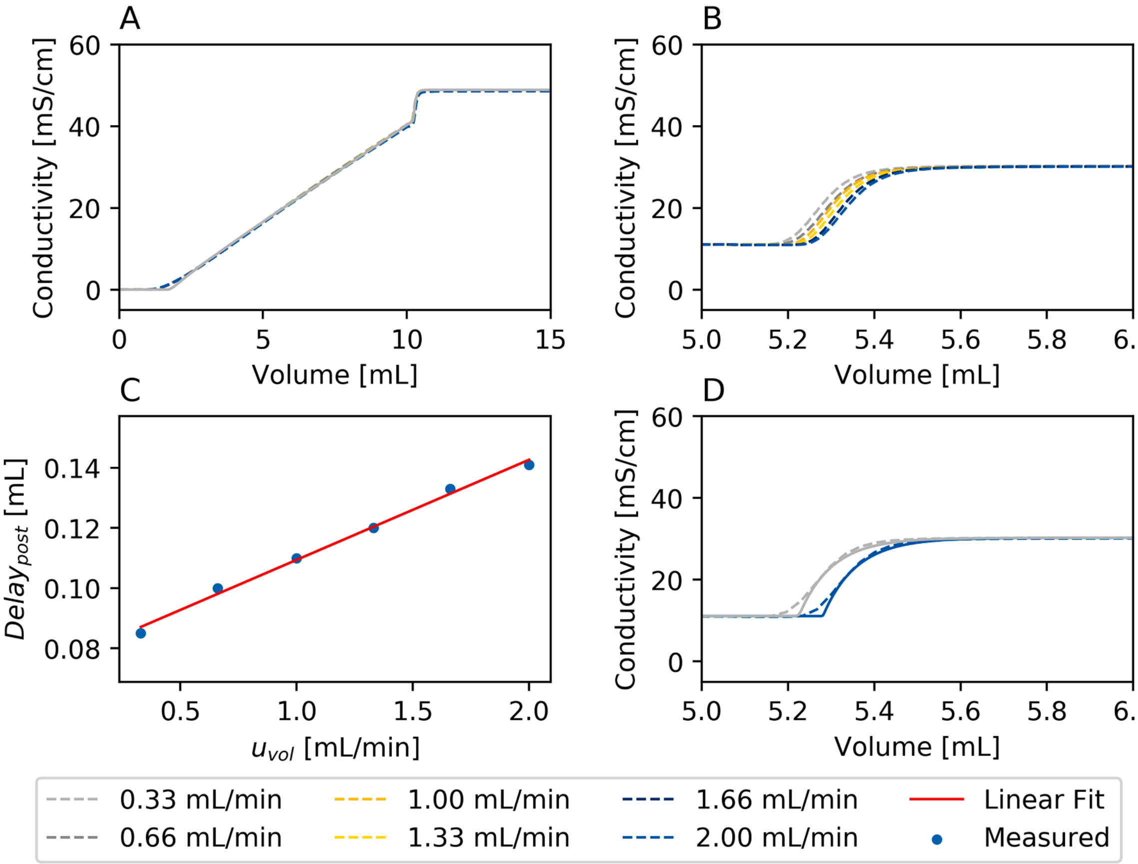

Fig. 2. Characterization of the ÄKTA Pure 25 system used in this study. (A) Conductivity traces of a 10 mL linear gradients at 0.33 – 2.00 mL/min (dashed lines) and a simulated conductivity trace (solid line). (B) conductivity traces used for characterization of $CSTR_{post}$ and $delay_{post}$ at flow rates ranging from 0.33 – 2.00 mL/min. (C) Flow dependent $delay_{post}$ and the linear fit with $delay_{post}$ = 0.033 min * u_{vol} + 0.076 mL (R^2 = 0.9935). (D) Overlay of measured and simulated post column conductivity traces at the maximum (2.00 mL/min) and minimum flowrate (0.33 mL/min) used for characterization.

In this study, a micro scale column was used to keep dispersive effects low and thereby preserve comparatively high UV signals that can be discriminated from signal noise and artifacts by switching of valves or matrix buffers. The total porosity ε_t and interstitial porosity ε_b were experimentally determined using acetone as pore penetrating tracer and MVP under non-binding conditions. Ionic capacity Λ was calculated from information of the vendor. D_{app} was calculated according to the empiric correlation described by Schweiger et al. [31] as described in *Section 3.4*. All column parameters are summarized in Table 2.

4.2. AEX chromatography profiles

After system and column characterization, the next step was to investigate the adsorption behavior of MVP to QSFF. The focus was on calibrating a mechanistic model capable of predicting the LRV of MVPs applied to a QSFF column in flowthrough mode. To determine the equilibrium constant k_{eq} and characteristic charge ν three LGE runs using sodium chloride as eluent were performed at lengths of 50, 100 and 150 CV. Shallow gradients and an asymmetric sampling were chosen for the LGEs to resolve the desorption of MVPs on the $\log_{10}$ scale. An additional ISE gradient with 20 mM sodium chloride increments ranging from 120 −240 mM sodium chloride was performed to allow for better estimation of the kinetic parameter k_{kin}.

As shown in Fig. 4A-C, during the LGE experiments the MVP eluted with a single peak of approximately 20 – 50 mAU at conductivities between 25 – 26 mS/cm corresponding to sodium chloride concentration of 248 – 260 mM. Across the LGE runs, the retention of elution peaks shifted towards lower sodium chloride concentrations. Subsequent Immuno-qPCR revealed that the concentration of MVP increased rapidly at the onset of the elution peak. However, the desorption of MVP could be resolved at $\log_{10}$ scale for shallower gradients by increasing the resolution of collected fractions at the onset of the elution. ISE showed ~ 2 mAU UV peaks that were barely distinguishable from signal noise at 200 mM and 220 mM sodium chloride (21 and 23 mS/cm). A better resolution for the ISE was given by the Immuno-qPCR analytics, which revealed that desorption of MVP starts at 140 mM (16 mS/cm) sodium chloride, where 2.2×10^6 MVP/mL were detected. In the following steps the MVP concentrations increased reaching the highest concentration of 2.9×10^9 MVP/mL at 200 mM and 220 mM (21 – 23 mS/cm) sodium chloride (Fig. 4D). For LGE and ISE runs, which were loaded with concentrations of 2.0×10^{10} MVP/mL, breakthroughs ranging from 2.5×10^6 – 5.6×10^6 MVP/mL were observed in the flowthrough/wash fraction.

For appropriate modeling of the MVP behavior both signals, the UV trace as well as the Immuno-qPCR, were necessary. The UV signal was considered to inform the model about the accurate position of the elution peak, while Immuno-qPCR was needed to quantitatively resolve the MVP desorption on the $\log_{10}$ scale.

4.3. Model calibration

The equilibrium constant k_{eq} and characteristic charge ν of the SMA isotherm were initially estimated from the peak positions of the UV traces of LGE runs, using the method described by Yamamoto et al. [35]. The kinetic parameter k_{kin} was determined from LGE and ISE runs with the inverse method of the GSCM software, using an adaptive simulated annealing algorithm. After initial calibration, immuno-qPCR results were added to the dataset. For refinement of the model parameters k_{eq}, ν

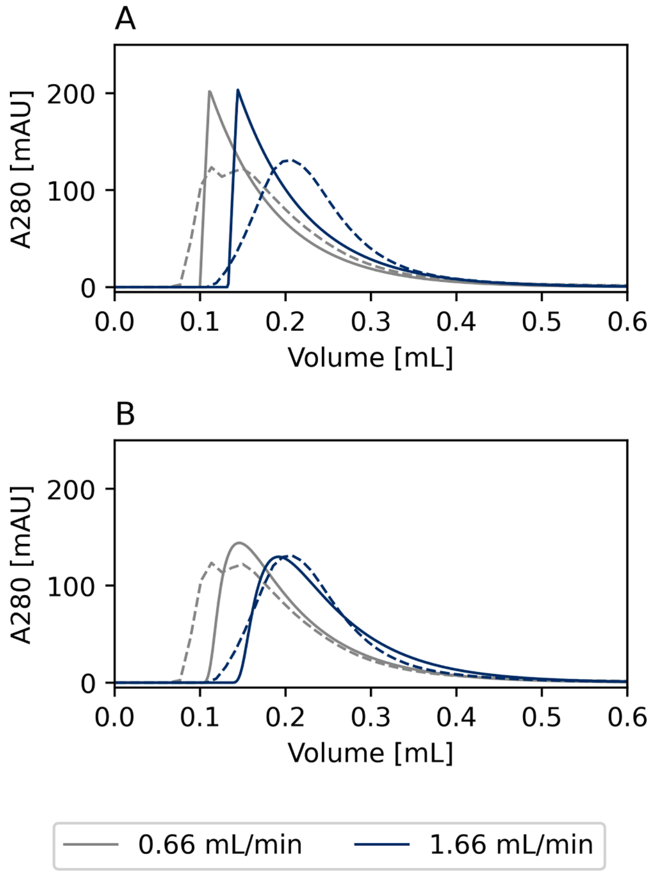

Fig. 3. Comparison of measured (dashed line) and simulated (solid line) band profiles of MVP pulses at 0.66 mL/min and 1.66 ml/min. (A) Before implementation of DPFR into the simulated system. (B) After implementation of DPFR into the simulated system.

Table 2
Column parameters, units, and sources.

Parameter	Symbol	Value	Unit	Source
Diameter	d_c	5	mm	Manufacturer
Length	L_c	10	mm	Manufacturer
Adapter volume	–	0.036	mL	[34]
Column volume	V_c	0.196	mL	$V_c = \pi\left(\frac{d_c}{2}\right)^2 L_c$
Bead radius	r_p	45	µm	Manufacturer
Fluid volume	V_f	0.174	mL	Pluse injection with acetone
Interstitial volume	V_{int}	0.104	mL	Pulse injection with MVP in 1 M NaCl
Total column porosity	ε_t	0.893	–	$\varepsilon_t = \frac{V_f}{V_c}$
Interstitial porosity	ε_b	0.534	–	$\varepsilon_b = \frac{V_{int}}{V_c}$
Axial dispersion	$D_{app.\ const}$	1.16×10^{-5}	mm^2/s	[31,32],
	$D_{app,\ lin}$	3.885		
	$D_{app,\ sqrd.}$	5.360		
Ionic capacity	Λ	1.60	M	$\Lambda = \frac{c_{Cl\_}\ V_{Cl\_}}{V_c(1-\varepsilon_t)}$

and k_{kin} a Levenberg-Marquardt algorithm was used. The shielding factor σ was assumed to be negligible and set to 0, based on a fractional surface coverage of 1.55 %, which was calculated as the ratio of the circular area of the MVP $A_{MVP} = \pi r_h^2 c_{MVP} V_{load}$ and the available particle surface $A_s = \frac{3}{r_p}(1-\varepsilon_b)A_c L_c$ obtained from Schmidt-Traub et al. [32], assuming the MVP does not enter the pores of the chromatography resin. Errors of the immuno-qPCR data were weighted twice over the UV traces. The SMA parameters estimated with the normalized L1 error function are shown in Table 3 including the 95 % confidence interval of the respective parameters.

In general, the peak positions and MVP concentrations of the LGE runs were well represented by the calibrated model. The simulation indicated that MVP desorption starts at slightly lower sodium chloride concentrations in the gradient. ISE runs showed high comparability of the measured and simulated MVP concentrations for the 120 to 220 mM (14 – 23 mS/cm) sodium chloride steps. For sodium chloride concentrations of 240 mM (24 mS/cm) and higher the simulation showed a considerably faster decline in eluting MVPs than the measurements (Fig. 4A-D). This was not considered as being critical since the main purpose of the model was to predict LRVs of AEX chromatography in flowthrough mode, where the initial decline of adsorbed MVP with increasing sodium chloride concentrations is more relevant. Overall, taking into account the challenges of accurately predicting the desorption of MVPs over a logarithmic range of concentrations, the variations between predictions and measurements were considered as acceptable.

4.4. Model verification: impact of sodium chloride concentration

To verify the capability of the calibrated model to predict MVP removal at different sodium chloride concentrations, flowthrough runs were simulated in 1 mM increments with sodium chloride concentration ranging from 0 to 400 mM. LRVs were calculated from simulated load and flowthrough concentrations as given in Eq. (7). As shown in Fig. 5, the simulation predicted a maximum LRV of 2.75 for sodium chloride concentrations < 98 mM and predicted a decrease of the LRV onwards until the LRV reached values < 0.01 at a sodium chloride concentration of 238 mM. 95 % confidence bands of the simulation appear to be wider at higher LRVs due to the representation of logarithmic values. It was assumed that the range of sodium chloride concentrations where LRVs decline rapidly represent the most challenging conditions. Therefore, verification runs were performed at sodium chloride concentrations from 120 to 240 mM. Additionally, one run was performed with 20 mM sodium chloride to examine whether the prediction is still valid at the lowest sodium chloride concentration applied in this study. In general, the simulated and measured LRVs showed a high comparability. LRVs for moderate and ineffective removal showed mainly overlapping confidence bands of the simulation and measurements. As observed during calibration of the model even at low sodium chloride concentrations, the LRV did not reach values of ≥ 4 $\log_{10}$ neither in the simulations nor in the measurements.

4.5. Model verification: impact of residence time

During mechanistic model calibration and small-scale verification, MVP breakthroughs were observed during the load and wash phase. This result was surprising since QSFF is known to effectively clear MVP at similar counterion concentrations [20,36]. It was assumed that these breakthroughs were caused by the short residence time of 18 s, resulting from the linear flowrate u_{lin} of 200 cm/h and L_c of 1 cm. This hypothesis was examined in silico *by* 200 flowthrough experiments simulated at residence times of 1 to 200 s. As shown in Fig. 6, simulations predicted a decline of LRV towards low residence times exceeding an LRV of 4 at 31 s. To verify the simulations, flowthrough experiments were performed at residence times of 7.2, 18.0, 24.0, 36.0, 72.0, and 144.0 s. The simulated and measured data showed a comparable behavior. Measured LRV declined down to 2.01 ± 0.19 $\log_{10}$ at 7 s residence time, while MVP was removed to a concentration below the LOQ for residence times of > 72.0 s resulting in LRVs $\geq 4.26 \pm 0.15$ $\log_{10.}$

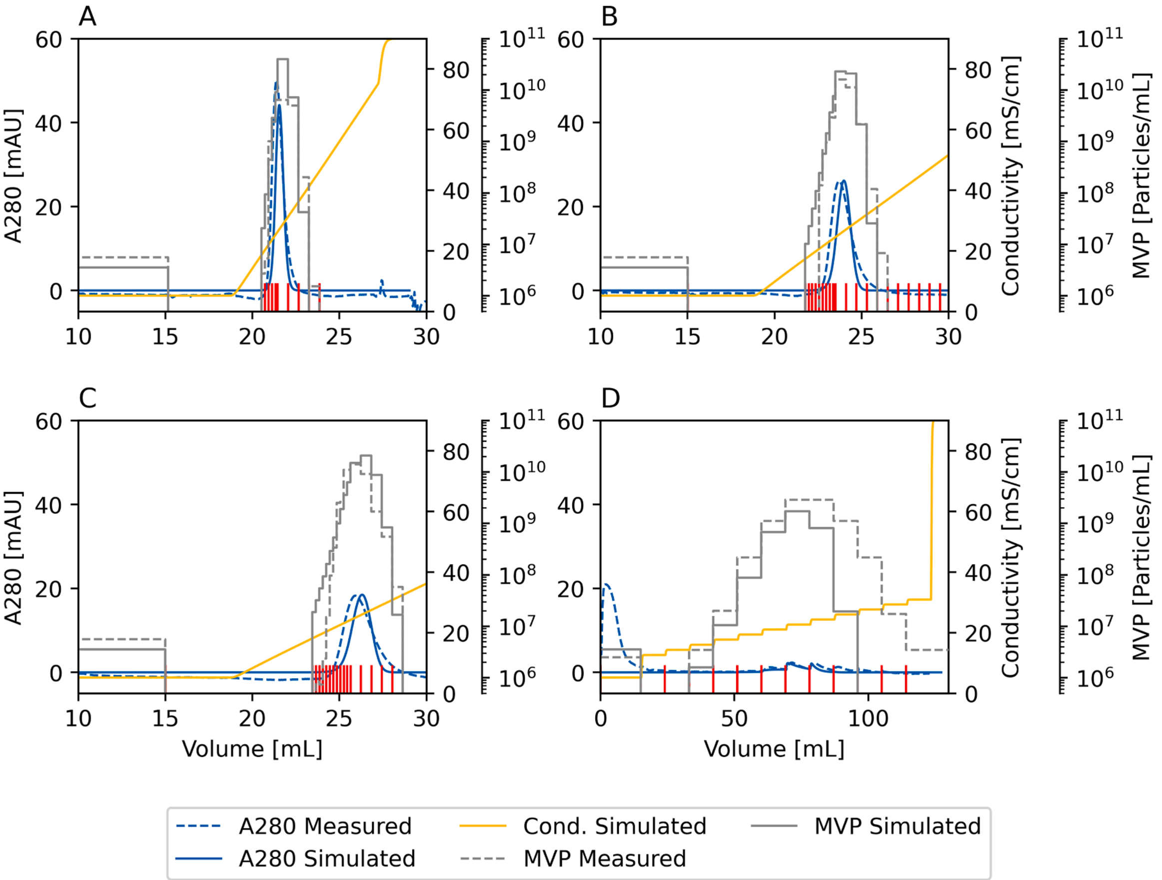

Fig. 4. Comparison of experimental (dashed lines) and simulated (solid lines) chromatograms of the chromatography runs used for calibration of (A) LGE 50 CV (B) LGE 100 CV (C) LGE 150 CV and (D) ISE chromatography runs used for calibration. Red horizontal streaks indicate fractions. MVP concentrations are shown on the $\log_{10}$ scale.

Table 3
SMA model parameters of the calibrated MVP model.

Parameter	Symbol	Value
Equilibrium constant [-]	$log_{10}(k_{eq,\ MVP})$	−11.48 ± 0.39
Kinetic coefficient [sM^{ν}]	$log_{10}(k_{kin,\ MVP})$	−8.49 ± 0.23
Charge [-]	ν_{MVP}	17.43 ± 0.55

4.6. In silico analysis of combined effects of sodium chloride and residence time on LRV

After verification of the mechanistic model in terms of sodium chloride and residence time dependencies of LRV, an *in-silico* analysis was performed to evaluate the interaction of both parameters. To do so, LRV over sodium chloride concentrations ranging from 0 to 400 mM were simulated at six residence times of 10, 20, 30, 40, 80 and 120 s.

As expected, based on the previous verification runs, longer residence times led to an increase in LRV even at low sodium chloride concentrations (Fig. 7). Further, this also impacted the slope of the transition from effective LRVs >4 to insignificant LRVs (< 1). During simulation at 10 s residence time, the LRV started to decline at ~ 140 mM, while at 120 s a potentially measurable decline of LRV was predicted for ~160 mM.

5. Discussion

5.1. System and column characterization

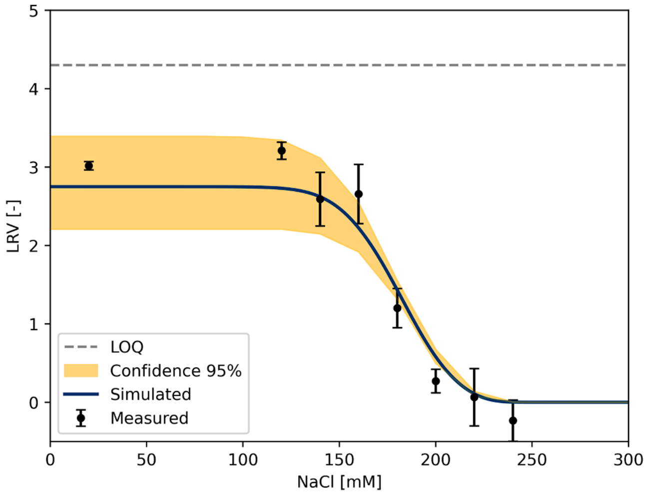

Fig. 5. Sodium chloride LRV relation predicted by the calibrated mechanistic model and measured LRVs from flowthrough chromatography verification runs. The shaded area shows the 95 % confidence band of the simulations, which is based on a sampling of the model parameter covariance matrix. Error bars of LRVs indicate the 95 % confidence intervals of Immuno qPCR measurements ($n = 3$). LRV LOQ is indicated in gray dashed line and was calculated from the load and LOQ of the MVP Immuno-qPCR.

For this study, a mechanistic model of a MVP was calibrated to predict virus clearance behavior of this particle on a QSFF column. To obtain sufficient UV signals for the calibration of the mechanistic model, a micro scale column was used. It is known that extra column effects on

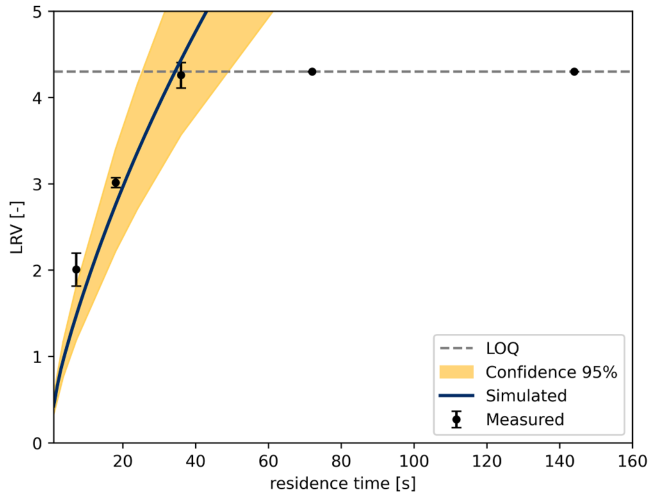

Fig. 6. Residence time LRV relation predicted by the calibrated mechanistic model and measured LRVs from flowthrough chromatography runs. The shaded area shows the 95 % confidence band of the simulations, which is based on a sampling of the model parameter covariance matrix. Error bars of LRVs indicate the 95 % confidence intervals of Immuno qPCR measurements ($n = 3$). LRV LOQ is indicated in gray dashed line and was calculated from the load and LOQ of the MVP Immuno-qPCR.

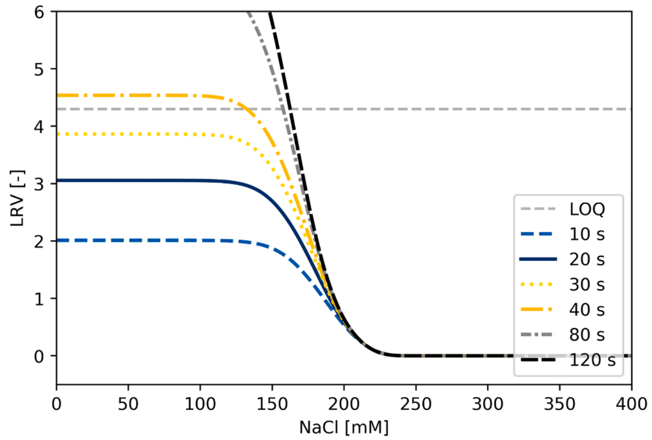

Fig. 7. Simulated LRV at different sodium chloride concentrations and residence times. LRV LOQ is indicated in light gray dashed line and was calculated from the theoretical load and LOQ of the MVP Immuno-qPCR.

the peak broadening become dominant for these types of columns, due to their small volumes [31]. Therefore, the system was characterized using sodium chloride as small molecule tracer to separate extra column band broadening from that related to the actual column. Additionally, the impact of different flow rates on extra column effects was examined. System mixing behavior was well described by adding $CSTR_{post}$ after the column. The mixing behavior of $CSTR_{post}$ was not flow-dependent but the system delay was linearly correlated to the volumetric flowrate u_{vol}. This linear behavior suggests that the effect was mainly caused by the pump regulation time of the used ÄKTA system. Similar observations have already been made for these types of system [33]. Although the use of sodium chloride as a tracer provided a good description of the system dispersion for small molecules it did not sufficiently describe the dispersive behavior of the MVP. Therefore, additional pulse experiments were performed, and a DPFR was added to the simulated system. The peak at the lower flow rate showed deformation at its onset. Similar behavior has been reported previously and is related to non-uniform distribution in the radial direction of tubing caused by the low diffusivity of large molecules [37,38]. One flow independent dispersion coefficient was sufficient to describe dispersion of MVP pulses at both flow rates. Although this might be surprising since higher flow rates in straight tubing are known lead to higher dispersion, Filip et al. showed that higher flow rates also lead to stronger turbulences in curved elements of the system, which contradict axial dispersion in straight tubing [39,40]. This effect might have contributed to the comparable dispersive behavior observed at the two different flow rates.

The porosity values of the column with ε_t of 0.893 and ε_b of 0.543 showed similar total porosity, but a slightly higher bed porosity compared to previously published values for QSFF with ε_t of 0.900 and ε_b of 0.310 [41]. ε_b for micro scale columns up to 49 % and high uncertainty have been shown [42,43]. High porosity values in small columns might lead to implications for scaling, due to strong effects of porosities on peak shapes [43,44]. However, this was considered as an acceptable tradeoff for MVP model calibration, since larger column types led to UV signals < 15 mAU (data not shown) when MVP concentrations were applied in ranges that are also feasible for viral clearance studies with infectious virus.

To estimate the flow dependent dispersion of the micro scale column the empirical correlation between column dimension, superficial velocity and intra column band broadening described by Schweiger et al. was used. This correlation relies on a broad dataset with minichrom columns and is based on pulses with the pore penetrating tracer acetone [31]. Usually, acetone tracers disqualify as tracer for axial dispersion due to their mass transfer into pores of the chromatography medium. However, Iurashev et al. showed that the effect of mass transfer becomes negligible for small columns as the micro scale column typeat the flow rates used in this study [34]. Therefore, it was assumed that deriving dispersive behavior from the empiric correlation published by Schweiger et al. provides a sufficient approximation.

5.2. Model calibration and verification

A mechanistic model for the removal of MVP with QSFF was calibrated to examine the applicability of such models to predict LRVs. An LKM was selected as the column model, while the SMA isotherm was used to model MVP adsorption. LKM models assume that film diffusion as well as intraparticle diffusion can be neglected. This assumption was made due to large size and low pore accessibility of the MVPs, and is similar to column models that have been developed for adeno-associated virus (AAV) purification [45,46]. Both AAV and MVM (the infectious pendant to the MVP) belong to the *parvoviridae* family and might show similar behavior during chromatography due to their similarities in structure and size [47]. Although this column model reduces the number of parameters to be fitted and experiments needed for calibration, it must be stated that the LKM lumps several non-idealities of the system into the parameter k_{kin}, including film diffusion, pore diffusion, adsorption kinetics, and extra column effects. This could lead to implications during scaling were the interplay between effects of the lumped parameters might change. Thus, more complex column models like transport dispersive lumped rate or even general rate models, that break down these physical phenomena, should also be taken into consideration when a scale up of the model is intended.

For model calibration three LGE runs and an ISE run were performed. Similar to previous observations [20,36] MVP eluted at sodium chloride concentrations of 200 mM and higher depending on the respective experiment. The peaks of the LGE runs were well distinguishable while ISE runs showed peaks with a relatively low absorption of ~2 mAU. The small peaks might be attributed to the small difference in sodium chloride concentrations, resulting in slow and only partial elution at each step. This highlights the importance of performing blank runs to distinguish the low MVP signals from artifacts introduced by noise or artifacts caused by the hardware used e.g. switching of valves. Based on the UV traces a workflow as it is typically used for proteins was applied, using Yamamoto's method for initial estimation of equilibrium constant

k_{eq} as well as characteristic charge ν and reverse estimation of kinetics k_{kin} from all calibration runs. Despite giving a good estimation for the UV profile and peak position it was necessary to immuno-qPCR measurements to the calibration dataset and refine of the model parameters to accurately describe the $\log_{10}$ scale. The poor description of MVP behavior alone was probably caused by the limitation of the UV signal. Although UV is good at detecting proteins and VLPs, it did not have enough sensitivity to resolve MVP behavior on the $\log_{10}$ scale, where small changes of the model parameters can have a considerable impact. In other words, an LRV of ~3 means that ~0.1 % of the particles initially spiked can be found in the flowthrough. Therefore, both the UV signal and a method with high sensitivity should be combined when it is intended to describe virus removal on a logarithmic scale.

The characteristic charge ν of 17.43 ± 0.55 and the equilibrium constant $\log_{10}$ ($k_{eq,\ MVP}$) of −11.48 ± 0.39 obtained during calibration were in ranges which are comparable to ranges that have been observed for other parvovirus types [45,46]. The kinetic constant $\log_{10}$ ($k_{kin,\ MVP}$) of −8.49 ± 0.23 was relatively small, thereby indicating a relatively fast kinetics. This was counterintuitive assuming slow diffusion of macromolecules like the MVP modeled in this study and might be caused by two circumstances. First, k_{kin} of the chosen LKM is not only accounting for diffusion limitations but also describing the adsorption kinetics. Second, a kinetic version of the SMA model was used. In this model k_{kin} and k_{eq} of the i th solute are defined as $k_{eq,i}=k_{ads,i}/k_{des,i}$, and $k_{kin,i} = 1/k_{des,i}$ respectively. A relatively small value of for k_{eq} was estimated. k_{kin} is inversely connected to the desorption rate k_{des}. When rearranging for k_{des}, a relatively fast value of 3.09×10^{8} can be calculated, while a adsorption rate k_{ads} of 1.02×10^{-3} is obtained. Therefore, the adsorption rate is relatively slow, which was necessary to describe the moderate breakthrough of MVP during load

Since relatively small errors can have a high impact on the LRV, it was critical to assess the confidence intervals of the estimated parameters after calibration. The confidence intervals of k_{eq}, k_{kin} *and* ν were comparatively narrow indicating that these parameters were well determined. This might be attributed to the selected modeling workflow consisting of asymmetrically sampled LGE runs with shallow gradient slopes and a ISE run. The high resolution at the onset of LGEs facilitated high confidence for peak position and thereby k_{eq} and ν. The ISE led to several peaks, which were hard to describe by the chosen mechanistic model and narrowed down the range of k_{kin}. Further, changes of k_{kin} had an impact on the simulated breakthrough of MVP thereby considering the MVP flowthrough for model calibration contributed to the high confidence of this parameter.

The major objective of the model was to predict the removal of MVP of QSFF at different sodium chloride concentrations. Therefore, eight flowthrough experiments unrelated to the calibration dataset were performed and compared to MVP removal predicted by the mechanistic model. The LRVs obtained from these experiments showed a decline of LRV in a similar range as the model and overlapping 95 % confidence intervals.

Further, the capability of the model to predict the impact of residence time on the removal was evaluated. In line with the simulations, the experimental data did not show effective LRV > 4 at 18.0 s of residence time. This was surprising since QSFF is known for its effective removal of MVM and MVP [21,36]. Reported data were either generated in a high throughput setting or using lab scale columns. Therefore, we assumed the observed LRVs were caused by a limitation of the micro scale columns used. Throughout this study, a linear flow rate u_{lin} of 200 cm/h, which is typically applied to lab scale and manufacturing columns, was used. This u_{lin} resulted in a residence time of 18 s on the micro scale columns. Interestingly, flow-dependent elution and absorption behavior have been reported for membrane and fibro chromatography devices [33,48]. Therefore, it was hypothesized that the MVP removal might be limited by the short residence time applied. To examine this hypothesis, simulations were performed at residence times between 1 – 200 s and verified with flowthrough experiments. Both showed a decline of LRV with shorter residence times, although a calculated fractional surface coverage of 1.55 % indicates that the steric factor should not be limiting. In this study, it was assumed that the mass transfer by interparticle diffusion can be neglected due the low participation of the MVP in the pore volume. Following this argumentation, the flowrate dependence of the MVP reduction might not be limited by mass transfer but by the adsorption kinetics k_{kin} and diffusion of comparatively large biomolecules like virus-like particles. Slow adsorption kinetics to Q-functionalized surfaces have been shown for several bacteriophages. Nevertheless, these kinetics were not critical for membrane adsorbers for u_{lin} up to 900 cm/h [49]. However, with increasing flow rates the slow adsorption rate k_{ads} discussed above may become limiting at the short residence times and comparatively high virus particle load densities applied in this study. This indicates that an increased flow rate can lead to decreased MVP clearance when extreme conditions such as short column size, low pore accessibility and high flow rates are combined.

However, it needs to be stated that a combination of such parameters hardly occurs when working with typical lab scale columns that keep the column length constant and are scaled by diameter. These columns usually have longer residence time of > 180 s, which results in effective MVP clearance (LRV > 4) according to the predictions of the verified model (c.f. Fig. 7).

6. Conclusion

In this study, we successfully used mechanistic modeling as a tool to predict the capability of QSFF to clear an MVP. A LKM was used to take the low pore accessibility of the MVP into account while counter ions were considered using an SMA isotherm. Due to the small column used the chromatography system was thoroughly characterized and mixing behavior was lumped into $CSTR_{pre}$, $CSTR_{post}$ and a DPFR. The characteristic charge ν, equilibrium constant k_{eq} and kinetic constant k_{kin} were initially estimated from UV traces of three LGE runs using Yamamoto method and one ISE run and subsequently refined using Immuno-qPCR data. Asymmetric sampling of LGE runs and the ISE run led to low model uncertainty, which was critical to make accurate predictions on the $\log_{10}$ scale. Subsequent verification runs showed that the model was capable of accurately predicting LRV at sodium chloride concentrations ranging from 0 to 400 mM.and residence times ranging 1 to 200 s. After verification the interplay between both parameters was extrapolated showing that flow dependent virus particle breakthrough becomes unlikely at residence times usually used during virus clearance studies, a finding that might be significant for the design of effective downstream unit operations. Since the applied modeling workflow mainly focused on generating resolution on the logarithmic scale, it might be also suited for other virus types e.g. infectious MVM, Retrovirus Like Particles, Murine Leukemia Virus, Reovirus-3 and impurities where this level of accuracy is needed.

In general, simulations with such a predictive power could be very useful to define acceptable range limits for critical process parameters (CPPs) and thereby enable the application of quality by design (QbD) principles to virus clearance. Further, an enhanced mechanistic understanding might enable application of prior knowledge to the evaluation of viral clearance of AEX chromatography. This concept has been introduced in ICHQ5a (R2) and enables platform validation instead of product specific validation of viral clearance. Although, this platform validation is currently limited to well understood and dedicated virus clearance steps (e.g. low pH inactivation or virus filtration), the Annex 5 of the ICHQ5a guideline also states that “based on evolving process understanding, further process steps may be considered for platform validation in the future” [6].

However, to achieve the proposed applications there are still some open challenges that have not been addressed in this study. Despite showing that mechanistic models can predict the impact of process parameters on clearance of viral particles, the influence of protein solutions and impurities (e.g. HCP, DNA) as well as scalability of this model were not examined. Since these parameters can have a significant impact on virus removal they should be addressed by future work.

Summarizing, models like this could enhance the mechanistic understanding of viral clearance. Thereby, such mechanistic models could contribute to the development of more efficient and safer biopharmaceutical downstream processes and might even enable a reduced number of validation runs by facilitating platform validation.

CRediT authorship contribution statement

Lukas Döring: Writing – review & editing, Writing – original draft, Visualization, Validation, Software, Methodology, Investigation, Formal analysis, Data curation, Conceptualization. **Johannes Winderl:** Writing – review & editing, Validation, Supervision, Software, Methodology, Conceptualization. **Matthias Kron:** Writing – review & editing, Supervision, Project administration, Funding acquisition, Conceptualization. **Jürgen Hubbuch:** Writing – review & editing, Supervision, Conceptualization.

Declaration of competing interest

The authors declare that they have no known competing financial interests or personal relationships that could have appeared to influence the work reported in this paper.

Data availability

Data will be made available on request.

Funding

This research did not receive any specific grant from funding agencies in the public, commercial, or not-for-profit sectors.

Acknowledgements

The authors would like to thank Thilo Grob and Dietmar Lang for making this study possible, and the whole process and analytical science for their support and the always constructive discussions.

References

[1] D. Saleh, G. Wang, F. Rischawy, S. Kluters, J. Studts, J. Hubbuch, In silico process characterization for biopharmaceutical development following the quality by design concept, Biotechnol. Prog. (2021) 37, https://doi.org/10.1002/btpr.3196.

[2] F. Rischawy, D. Saleh, T. Hahn, S. Oelmeier, J. Spitz, S. Kluters, Good modeling practice for industrial chromatography: mechanistic modeling of ion exchange chromatography of a bispecific antibody, Comput. Chem. Eng. (2019) 130, https://doi.org/10.1016/j.compchemeng.2019.106532.

[3] F. Rischawy, T. Briskot, N. Hopf, D. Saleh, G. Wang, S. Kluters, J. Studts, J. Hubbuch, Connected mechanistic process modeling to predict a commercial biopharmaceutical downstream process, Comput. Chem. Eng. (2023) 176, https://doi.org/10.1016/j.compchemeng.2023.108292.

[4] T. Hahn, N. Geng, K. Petrushevska-Seebach, M.E. Dolan, M. Scheindel, P. Graf, K. Takenaka, K. Izumida, L. Li, Z. Ma, N. Schuelke, Mechanistic modeling, simulation, and optimization of mixed-mode chromatography for an antibody polishing step, Biotechnol. Prog. 39 (2023) 1–13, https://doi.org/10.1002/btpr.3316.

[5] H. Shirataki, S.R. Wickramasinghe, Modeling virus filtration based on a multilayer membrane morphology and pore size distribution, Biochem. Eng. J. (2023) 194, https://doi.org/10.1016/j.bej.2023.108903.

[6] E.Medicines Agency, Committee for human medicinal products ICH guideline Q5A (R2) on viral safety evaluation of biotechnology products derived from cell lines of human or animal origin Step 2b, 2022. www.ema.europa.eu/contact.

[7] M. Dinowitz, Y.S. Lie, M.A. Low, R. Lazar, C. Fautz, B. Potts, J. Sernatinger, K. Anderson, Recent studies on retrovirus-like particles in Chinese hamster ovary cells, Dev. Biol. Stand. 76 (1992) 201–207. http://europepmc.org/abstract/MED/1282476.

[8] K.P. Anderson, Y.S. Lie, M.A. Low, S.R. Williams, E.H. Fennie, T.P. Nguyen, F. M. Wurm, Presence and transcription of intracisternal A-particle-related sequences in CHO cells, J. Virol. 64 (1990) 2021–2032, https://doi.org/10.1128/jvi.64.5.2021-2032.1990.

[9] G. Miesegaes, S. Lute, K. Brorson, Analysis of viral clearance unit operations for monoclonal antibodies, Biotechnol. Bioeng. 106 (2010) 238–246, https://doi.org/10.1002/bit.22662.

[10] O.O. Ajayi, S.A. Johnson, T. Faison, N. Azer, J.L. Cullinan, J. Dement-Brown, S. C. Lute, An updated analysis of viral clearance unit operations for biotechnology manufacturing, Curr. Res. Biotechnol. 4 (2022) 190–202, https://doi.org/10.1016/j.crbiot.2022.03.002.

[11] D.M. Strauss, S. Lute, K. Brorson, G.S. Blank, Q. Chen, B. Yang, Removal of endogenous retrovirus-like particles from CHO-Cell derived products using Q sepharose fast flow chromatography*, Am. Inst. Chem. Eng. Biotechnol. Prog. 25 (2009) 1194–1197, https://doi.org/10.1021/bp.249.

[12] D.M. Strauss, S. Lute, Z. Tebaykina, D.D. Frey, C. Ho, G.S. Blank, K. Brorson, Q. Chen, B. Yang, Understanding the mechanism of virus removal by Q sepharose fast flow chromatography during the purification of CHO-cell derived biotherapeutics, Biotechnol. Bioeng. 104 (2009) 371–380, https://doi.org/10.1002/bit.22416.

[13] D.M. Strauss, T. Cano, N. Cai, H. Delucchi, M. Plancarte, D. Coleman, G.S. Blank, Q. Chen, B. Yang, Strategies for developing design spaces for viral clearance by anion exchange chromatography during monoclonal antibody production, Biotechnol. Prog. 26 (2010) 750–755, https://doi.org/10.1002/btpr.385.

[14] A. Goyon, M. Excoffier, M. Claire JANIN BUSSAT, B. Bobaly, S. Fekete, D. Guillarme, A. Beck, Determination of isoelectric points and relative charge variants of 23 therapeutic monoclonal antibodies, 2017. http://www.elsevier.com/open-access/userlicense/1.0/.

[15] B. Michen, T. Graule, Isoelectric points of viruses, J. Appl. Microbiol. 109 (2010) 388–397, https://doi.org/10.1111/j.1365-2672.2010.04663.x.

[16] T. Iskra, A. Sacramo, C. Gallo, R. Godavarti, S. Chen, S. Lute, K. Brorson, Development of a modular virus clearance package for anion exchange chromatography operated in weak partitioning mode, Biotechnol. Prog. 31 (2015) 750–757, https://doi.org/10.1002/btpr.2080.

[17] M. Zhang, G.R. Miesegaes, M. Lee, D. Coleman, B. Yang, M. Trexler-Schmidt, L. Norling, P. Lester, K.A. Brorson, Q. Chen, Quality by design approach for viral clearance by protein a chromatography, Biotechnol. Bioeng. 111 (2014) 95–103, https://doi.org/10.1002/bit.24999/abstract.

[18] C. De Wit, C. Fautz, Y. Xu, Real-time quantitative PCR for retrovirus-like particle quantification in CHO cell culture, Biologicals 28 (2000) 137–148, https://doi.org/10.1006/biol.2000.0250.

[19] M. Hussain, W.J. Rayfield, D.J. Roush, A direct RT qPCR method for quantification of retrovirus-like particles in biopharmaceutical production with CHO cells, J. Pharm. Biomed. Anal. (2020) 189, https://doi.org/10.1016/j.jpba.2020.113472.

[20] J.D. Orchard, D. Cetlin, M. Pallansch, R. Barlow, J. Borman, A. Dhar, L. Pallansch, M. Dickson, Using a noninfectious MVM surrogate for assessing viral clearance during downstream process development, Biotechnol. Prog. 36 (2020), https://doi.org/10.1002/btpr.2921.

[21] S. Johnson, K.A. Brorson, D.D. Frey, A.K. Dhar, D.A. Cetlin, Characterization of non-infectious virus-like particle surrogates for viral clearance applications, Appl. Biochem. Biotechnol. 183 (2017) 318–331, https://doi.org/10.1007/s12010-017-2447-y.

[22] R. Dyer, Y. Song, J. Chen, E. Bigelow, J. McGinnis, L. Jenkins, S. Ghose, Z.J. Li, Mechanistic insights into viral clearance during the chromatography steps in antibody processes by using virus surrogates, Biotechnol. Prog. 36 (2020), https://doi.org/10.1002/btpr.3057.

[23] C. Pan, A. Becerra-Arteaga, B. Tran, M. Chinn, H. Wang, Q. Chen, H. Lutz, M. Zhang, Characterizing and enhancing virus removal by protein A chromatography, Biotechnol. Bioeng. 116 (2019) 846–856, https://doi.org/10.1002/bit.26866.

[24] T. Kayukawa, A. Yanagibashi, T. Hongo-Hirasaki, K. Yanagida, Particle-based analysis elucidates the real retention capacities of virus filters and enables optimal virus clearance study design with evaluation systems of diverse virological characteristics, Biotechnol. Prog. 38 (2022), https://doi.org/10.1002/btpr.3237.

[25] H. Feroz, D. Cetnar, R. Hewlett, S. Sharma, M. Holstein, S. Ghose, Z.J. Li, Surrogate model to screen for inactivation-based clearance of enveloped viruses during biotherapeutics process development, Biotechnol. J. 16 (2021), https://doi.org/10.1002/biot.202100176.

[26] M.R. Brown, S.A. Johnson, K.A. Brorson, S.C. Lute, D.J. Roush, A step-wise approach to define binding mechanisms of surrogate viral particles to multi-modal anion exchange resin in a single solute system, Biotechnol. Bioeng. 114 (2017) 1487–1494, https://doi.org/10.1002/bit.26251/abstract.

[27] J. Hung, S.F. Lam, Z. Tan, D. Choy, N. Chennamsetty, A. Lewandowski, W. Qi, M. Lynch, S. Ghose, Z.J. Li, Impact of virus-antibody interactions on viral clearance in anion exchange chromatography, J. Chromatogr. A. 1633 (2020), https://doi.org/10.1016/j.chroma.2020.461635.

[28] K. Brorson, H. Shen, S. Lute, J.S. Pérez, D.D. Frey, Characterization and purification of bacteriophages using chromatofocusing, J. Chromatogr. A. 1207 (2008) 110–121, https://doi.org/10.1016/j.chroma.2008.08.037.

[29] C.A. Brooks, S.M. Cramer, Steric mass-action ion exchange: displacement profiles and induced salt gradients, AIChE J 38 (1992) 1969–1978, https://doi.org/10.1002/aic.690381212.

[30] T Hahn, P Baumann, T Huuk, V Heuveline, J Hubbuch, UV absorption-based inverse modeling of protein chromatography, Eng Life Sci 16 (2) (2016) 99–106.

[31] S. Schweiger, A. Jungbauer, Scalability of pre-packed preparative chromatography columns with different diameters and lengths taking into account extra column effects, J. Chromatogr. A. 1537 (2018) 66–74, https://doi.org/10.1016/j.chroma.2018.01.022.

[32] H. Schmidt-Traub (Ed.), Preparative chromatography: of fine chemicals and pharmaceutical agents, Wiley-VCH, Weinheim, Germany, 2005, https://doi.org/10.1002/3527603484.

[33] T. Hahn, T. Trunzer, F. Rusly, R. Zolyomi, L.K. Shekhawat, G. Malmquist, A. Hesslein, H. Tjandra, Predictive scaling of fiber-based protein A capture chromatography using mechanistic modeling, Biotechnol. Bioeng. (2023), https://doi.org/10.1002/bit.28434.

[34] D. Iurashev, S. Schweiger, A. Jungbauer, J. Zanghellini, Dissecting peak broadening in chromatography columns under non-binding conditions, J. Chromatogr. A. 1599 (2019) 55–65, https://doi.org/10.1016/j.chroma.2019.03.065.

[35] S. Yamamoto, M. Nomura, Y. Sano, Adsorption chromatography of proteins: determination of optimum conditions, AIChE J 33 (1987) 1426–1434, https://doi.org/10.1002/aic.690330903.

[36] K.C. Gulla, Z.J. Schneiderman, S.E. O'Connell, G.F. Arias, N.L. Cibelli, D. Cetlin, D. B. Gowetski, High throughput chromatography and analytics can inform viral clearance capabilities during downstream process development for biologics, Biotechnol. J. (2021) 16, https://doi.org/10.1002/biot.202000641.

[37] A. Shankar, A.M. Lenhoff, Dispersion in round tubes and its implications for extra-column dispersion, 1991, J Chromatogr. A. 556 (1991) 235–248.

[38] K. Baran, W.K. Marek, W. Piątkowski, D. Antos, Effect of flow behavior in extra-column volumes on the retention pattern of proteins in a small column, J. Chromatogr. A. 1598 (2019) 154–162, https://doi.org/10.1016/j.chroma.2019.03.060.

[39] B. Filip, R. Bochenek, K. Baran, D. Strzałka, D. Antos, Influence of the geometry of extra column volumes on band broadening in a chromatographic system. Predictions by computational fluid dynamics, J. Chromatogr. A. (2021) 1653, https://doi.org/10.1016/j.chroma.2021.462410.

[40] B. Filip, R. Bochenek, W.K. Marek, D. Antos, Flow behavior of protein solutions in a lab-scale chromatographic system, J. Chromatogr. A. (2023) 1705, https://doi.org/10.1016/j.chroma.2023.464178.

[41] F. Steinebach, B. Coquebert de Neuville, M. Morbidelli, Relating saturation capacity to charge density in strong cation exchangers, J. Chromatogr. A. 1507 (2017) 95–103, https://doi.org/10.1016/J.CHROMA.2017.05.054.

[42] S. Schweiger, E. Berger, A. Chan, J. Peyser, C. Gebski, A. Jungbauer, Packing quality, protein binding capacity and separation efficiency of pre-packed columns ranging from 1 mL laboratory to 57 L industrial scale, J. Chromatogr. A. 1591 (2019) 79–86, https://doi.org/10.1016/j.chroma.2019.01.014.

[43] S. Schweiger, S. Hinterberger, A. Jungbauer, Column-to-column packing variation of disposable pre-packed columns for protein chromatography, J. Chromatogr. A. 1527 (2017) 70–79, https://doi.org/10.1016/j.chroma.2017.10.059.

[44] J. Koch, D. Scheps, M. Gunne, O. Boscheinen, C. Frech, Mechanistic modeling of cation exchange chromatography scale-up considering packing inhomogeneities, J. Sep. Sci. 46 (2023), https://doi.org/10.1002/jssc.202300031.

[45] J. Gomis-Fons, B. Zee, D. Hurwit, J. Woo, J. Moscariello, B. Nilsson, Mechanistic modeling of empty-full separation in recombinant adeno-associated virus production using anion-exchange membrane chromatography, Biotechnol. Bioeng. 121 (2024) 719–734, https://doi.org/10.1002/bit.28595.

[46] W.R. Keller, A. Picciano, K. Wilson, J. Xu, H. Khasa, M. Wendeler, Rational downstream development for adeno-associated virus full/empty capsid separation – A streamlined methodology based on high-throughput screening and mechanistic modeling, J. Chromatogr. A. (2024) 1716, https://doi.org/10.1016/j.chroma.2024.464632.

[47] M. Mietzsch, J.J. Pénzes, M. Agbandje-Mckenna, Twenty-five years of structural parvovirology, Viruses 11 (2019), https://doi.org/10.3390/v11040362.

[48] C. Ladd Effio, T. Hahn, J. Seiler, S.A. Oelmeier, I. Asen, C. Silberer, L. Villain, J. Hubbuch, Modeling and simulation of anion-exchange membrane chromatography for purification of Sf9 insect cell-derived virus-like particles, J. Chromatogr. A. 1429 (2016) 142–154, https://doi.org/10.1016/j.chroma.2015.12.006.

[49] M. Phillips, J. Cormier, J. Ferrence, C. Dowd, R. Kiss, H. Lutz, J. Carter, Performance of a membrane adsorber for trace impurity removal in biotechnology manufacturing, J. Chromatogr. A. 1078 (2005) 74–82, https://doi.org/10.1016/j.chroma.2005.05.007.